REPORT DOCUMENTATION PAGE

AFRL-SR-AR-TR-03-

0493

1. AGENCY USE ONLY (*Leave Blank*)	2. REPORT DATE August 31, 2003	3. REPORT TYPE AND DATES COVERED Final Technical, 08/02-05/03

4. TITLE AND SUBTITLE
New Approaches to High Power Microwave Computation and Experimentation
AFOSR New World Vistas Grant

5. FUNDING NUMBERS
F49620-00-1-0042 MS

6. AUTHORS
Edl Schamiloglu and Chaouki Abdallah

7. PERFORMING ORGANIZATION NAME(S) AND ADDRESS(ES)
University of New Mexico
Department of Electrical and Computer Engineering
Albuquerque, NM 87131-1356

8. PERFORMING ORGANIZATION REPORT NUMBER

9. SPONSORING / MONITORING AGENCY NAME(S) AND ADDRESS(ES)
AFOSR/NE
4015 Wilson Blvd, Room 713
Arlington, VA 22203-1954

10. SPONSORING / MONITORING AGENCY REPORT NUMBER

11. SUPPLEMENTARY NOTES

12a. DISTRIBUTION / AVAILABILITY STATEMENT
Unlimited
APPROVED FOR PUBLIC RELEASE,
DISTRIBUTION UNLIMITED

12b. DISTRIBUTION CODE
AFOSR/NE

13. ABSTRACT *(Maximum 200 words)*

This final technical report describes the conclusion of effort on the New World Vistas grant entitled "New Approaches to High Power Microwave Computation and Experimentation." In the final year of effort we focused on concluding studies of the radial acceletron, relativistic magnetron with axial extraction, cyclotron suppression in Cerenkov devices, and the development of components of interest to HPM. As an interesting application, we also investigated the use of HPM to propel payloads out of the solar system and proposed a means for communicating with such a payload.

14. SUBJECT TERMS
High power microwaves, radial acceletron, Bragg reflectors, cyclotron suppression
radial acceletron, Cerenkov sources, cyclotron suppression

15. NUMBER OF PAGES
30

16. PRICE CODE

17. SECURITY CLASSIFICATION OF REPORT	18. SECURITY CLASSIFICATION OF THIS PAGE	19. SECURITY CLASSIFICATION OF ABSTRACT	20. LIMITATION OF ABSTRACT
Unclassified	Unclassified	Unclassified	None

NSN 7540-01-280-5500

Standard Form 298 (Rev. 2-89)
Prescribed by ANSI Std. Z39-1
298-102

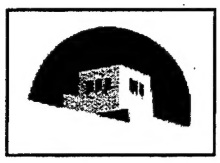

The University of New Mexico

Pulsed Power, Beams and Microwaves Laboratory, Department of Electrical & Computer Engineering

AFOSR New World Vistas: New Approaches to High Power Microwave Computation and Experimentation

Final Technical Report
1 August 2002 – 31 May 2003

31 August 2003

Submitted by:

Edl Schamiloglu — Principal Investigator and Professor
Department of Electrical and Computer Engineering
University of New Mexico
Albuquerque, NM 87131
Tel. (505) 277-4423
Fax: (505) 277-1439
e-mail: edl@ece.unm.edu

TABLE OF CONTENTS

INTRODUCTION

This final technical report describes work performed during the final period of effort on the New World Vistas grant entitled "New Approaches to High Power Microwave Computation and Experimentation." In the final year of effort we focused on concluding studies of the radial acceletron, relativistic magnetron with axial extraction, cyclotron suppression in Cerenkov devices, and the development of components of interest to HPM. We also investigated the use of HPM to propel payloads out of the solar system and proposed a means for communicating with such a payload (a very small exploratory effort). We provide a summary of these results, and extensive details can be found in the publication list.

LIST OF OBJECTIVES AND THEIR STATUS

Narrowband High Peak Power Sources

In this section we summarize the progress-to-date on our research related to high peak power narrowband sources.

A. Conclusion of Effort on Radial Acceletron

RF oscillators using radially propagating planar electron beams were initially proposed by Varian [1] in 1941, as part of the work undertaken at Stanford University during development of the klystron. Not recognized at the time were many of the advantages inherent in such a radial geometry:

- low electron source (diode) impedance due to the cylindrical geometry
- simplified coupling between the RF generating device and the output structure (cylindrical device to cylindrical waveguide or transmission line)
- simplified analysis and construction, due to entirely two-dimensional cylindrical geometry
- minimal or no external magnetic field required to control electron beam instabilities

The radial klystron work by Varian was entirely conceptual, and primarily contained (in outline form) in a patent application; the detailed analysis and experimental work to support the patent application was conducted primarily on klystrons of conventional design. Other than the initial theoretical work by Varian, RF generation using radially propagating planar electron beams remained largely unexplored until the early 1990's. At that time, as an outgrowth to work simulating a cylindrically symmetric millimeter-wave transit time oscillator, Arman [2] noted the advantages of a radially propagating planar beam and developed a proposal for a radial klystron oscillator [3] independent of the earlier work by Varian. The radial klystron oscillator was further refined into the radial acceletron: a cylindrically symmetric transit time oscillator propagating a planar electron beam radially in the anode-cathode (A-K) gap. The development work by Arman was done entirely numerically, using the $2^1/_2$D (2D geometry, 3D fields and particle motion) particle-in-cell (PIC) electromagnetic simulation code MAGIC [4].

Based on the promising simulation results by Arman, an experimental prototype was designed and fabricated. Although the original numerical analysis and design was done for a millimeter-wave device, the experimental prototype was designed to operate at approximately 3.1 GHz; this operating frequency was a consequence of the desire to have a physically large prototype in order to simplify fabrication and instrumentation. A comprehensive report on the details of this work can be found in [5]. Here we summarize the conclusions.

Overview and Summary of Results

The experimental results are presented here in logical order - not necessarily the order in which the actual experiment was conducted. In actuality the simulation and experimental efforts were closely coupled: as experimental data became available to compare with simulation predictions, errors and weaknesses in the simulation were identified and

corrected; and, improved simulation results obtained. The improved simulation predictions were subsequently used to modify the prototype design and experimental configuration. Initial cold tests were accomplished using classical technique: driving the cavity at frequency and measuring the system response. Do to the multiplicity of nearly-degenerate cavity modes, this classical method had little value. At the conclusion of the experiment, this cold testing was re-accomplished using B-dot probes to directly measure energy loss and energy storage as a function of frequency. With these measurements, cavity Q was calculated from first principles. The planar vacuum diode used as a load for the x-ray safety survey turned out to have considerable value: the measured diode perveance is a direct indication of simulation accuracy in predicting the radial acceletron diode current, and the effect of simulation instabilities on RF oscillation growth could be quantified. In general, the planar diode perveance closely matched that predicted by 1-D theory, and did not match the simulation predictions. The simulation-predicted 20 GHz RF oscillation was not seen during experiments. These same results were seen for test shots on the radial acceletron with the extractor not installed: diode perveance closely matched analytical theory, simulation-predicted perveance did not match either theory or experiment, and simulation predicted a high frequency (6 GHz) RF oscillation that wasn't seen experimentally. After revising the simulations to account for the initial data, simulation predicted that no RF would be seen in the radial acceletron for short (50 ns) voltage pulses; this is also what was observed experimentally. After modifying the Blumlein to allow a 300 ns voltage pulse, simulation predicted strong RF oscillation near the end of the voltage pulse; experimentally, only weak RF was observed. Further simulation indicated that the ferrite tile in the radial acceletron extractor region was likely strongly absorbing cavity RF, resulting in a significant reduction in Q. To minimize this problem, the extractor was extended 8 inches (20 cm) to a total length of 14 inches (35 cm). In this configuration, simulation predicted that strong RF would be observed beginning near the center of the 300 ns voltage pulse; experimentally, significant RF was not observed until the trailing end of the voltage pulse. The experimentally observed 3.2 GHz RF frequency was reasonably close to the simulation-predicted value of 3.3 GHz. As a final experiment, the ferrite tile was removed from the radial acceletron exit, and the system was fired into an anechoic chamber.; the intent was to try and measure the free-field radiation power using conventional techniques. As expected (and as predicted by simulation), the significant change in extractor termination impedance resulted in no significant RF being produced or radiated.

Estimation of cavity quality factor and the equivalent loss resistance 'R' was accomplished in two stages. As an initial step, MAGIC simulation was used to relate the cavity total stored energy to the RF field dB/dt at the locations of the cavity probes (B-dot probes 1, 2, 5, and 6); and to relate the RF energy loss rate to the input and output line dB/dt at the position of the extractor probes (B-dot probes 3 and 4). The cavity was then driven by an HP 8510C at the A-K gap, and the resulting fields at the probe locations measured. The calculated cold-cavity Q and R are shown in Figs. 1(a) –1(l), and compared to the simulation-predicted values. In general, nulls (regions of large losses) in the R and Q curves are well predicted by simulation. Both the positions and values of the peaks of the R and Q curves are not well predicted.

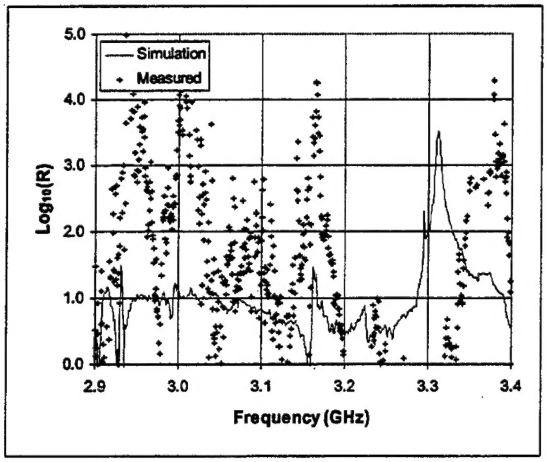

Figure 1(a). Equivalent resistance (R) for 7.0 cm extractor space.

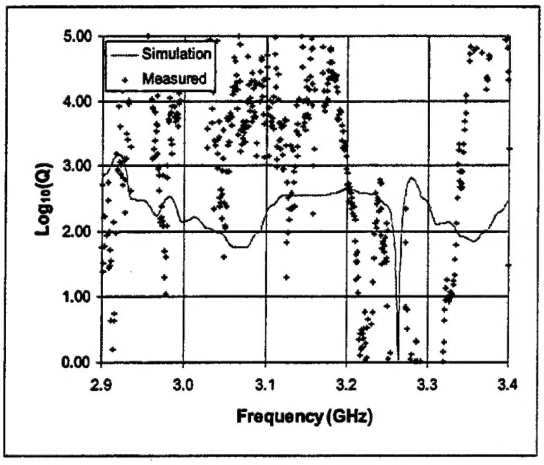

Figure 1(b). Cavity quality factor (Q) for 7.0 cm extractor space.

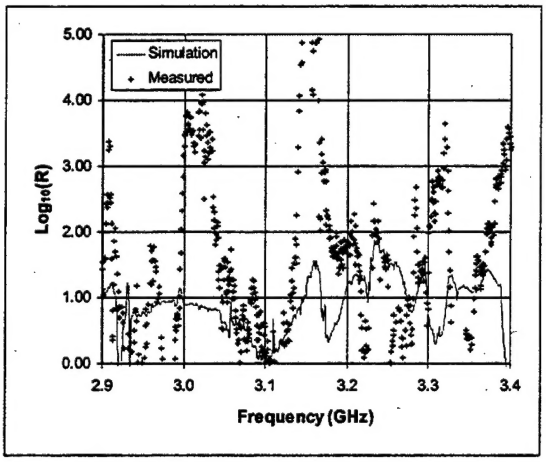

Figure 1(c). Equivalent resistance (R) for 7.5 cm extractor space.

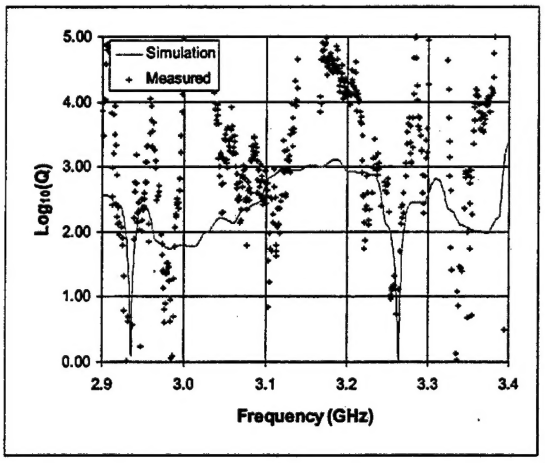

Figure 1(d). Cavity quality factor (Q) for 7.5 cm extractor space.

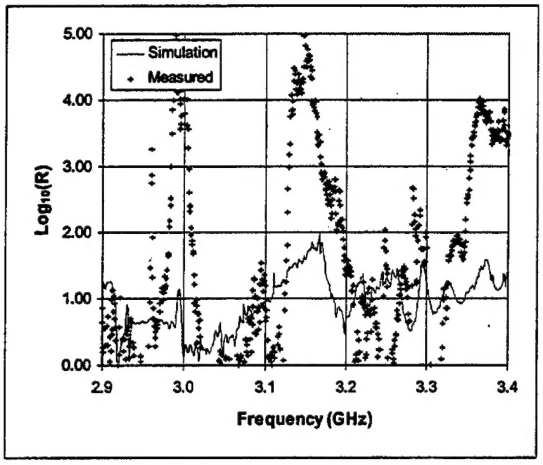

Figure 1(e). Equivalent resistance (R) for 8.0 cm extractor space.

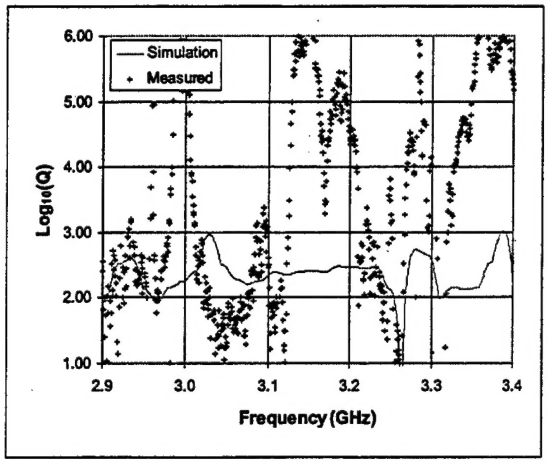

Figure 1(f). Cavity quality factor (Q) for 8.0 cm extractor space.

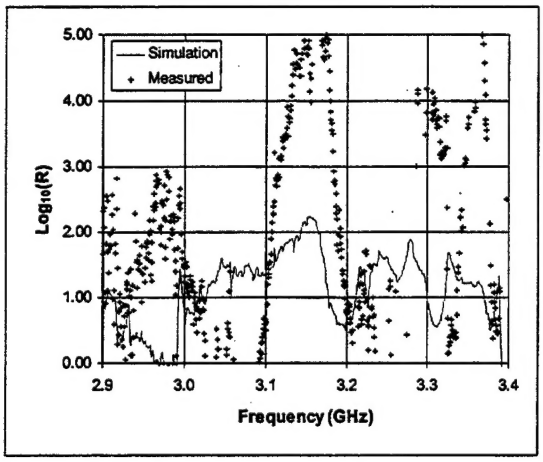

Figure 1(g). Equivalent resistance (R) for 8.5 cm extractor space.

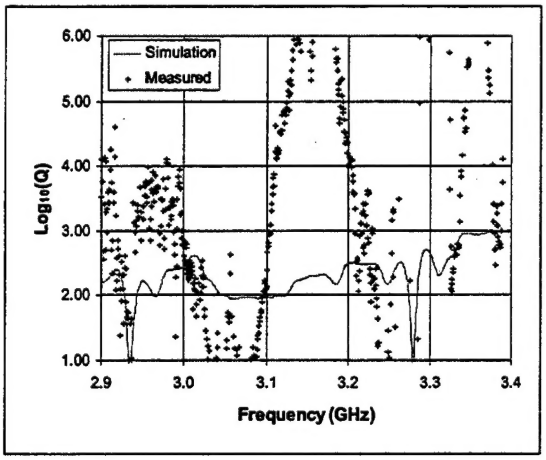

Figure 1(h). Cavity quality factor (Q) for 8.5 cm extractor space.

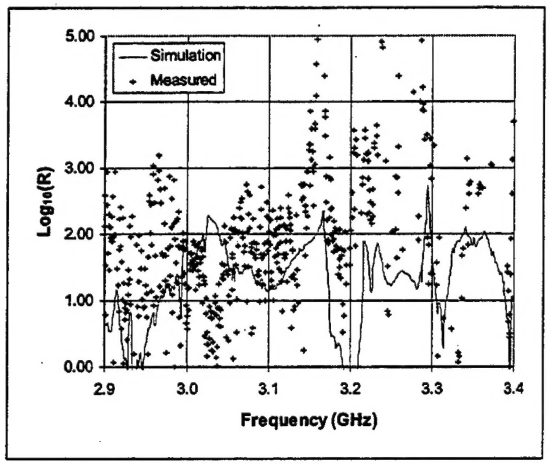

Figure 1(i). Equivalent resistance (R) for 9.0 cm extractor space.

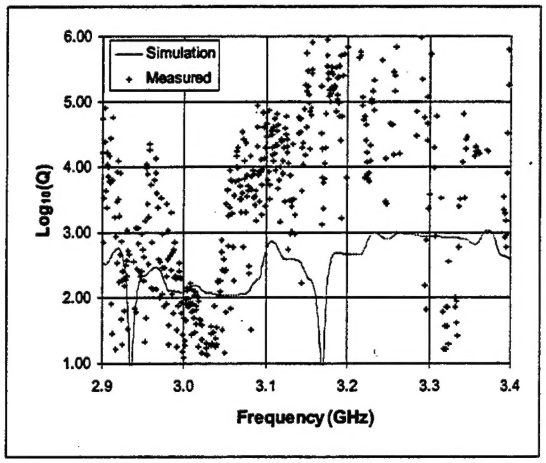

Figure 1(j). Cavity quality factor (Q) for 9.0 cm extractor space.

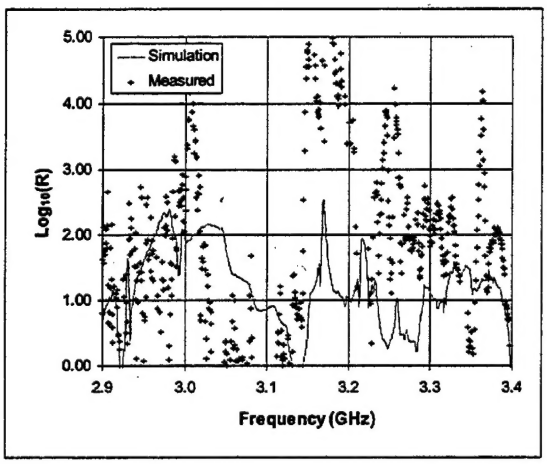

Figure 1(k). Equivalent resistance (R) for 9.5 cm extractor space.

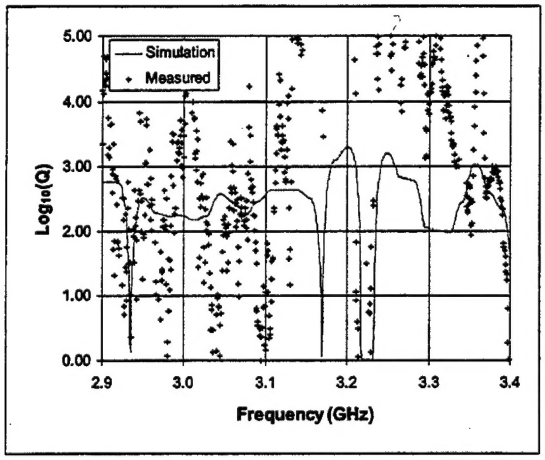

Figure 1(l). Cavity quality factor (Q) for 9.5 cm extractor space.

There are two possible explanations for the poor prediction accuracy: 1) approximation errors in the simulation mathematical formulation result in significant errors when estimating diffraction losses around sharp corners; and, 2) the actual termination of the extractor (ferrite tile) does not match the simulation-assumed perfect termination with no reflected RF. The measured data does not provide a method for distinguishing between these explanations.

The planar diode perveance as a function of pulse voltage is shown in Fig. 2. The measured values of diode perveance are well-predicted by the classic Child-Langmuir 1-D model (corrected for relativistic and edge effects); neither versions of the PIC simulation code are well matched to the experimental measurements.

The radial acceletron diode perveance as a function of pulse voltage is shown in Fig. 3. The measured values of diode perveance are well-predicted by the classic Child-Langmuir 1-D cylindrical-geometry model (corrected for relativistic and edge effects); neither versions of the PIC simulation codes are well matched to the experimental measurements.

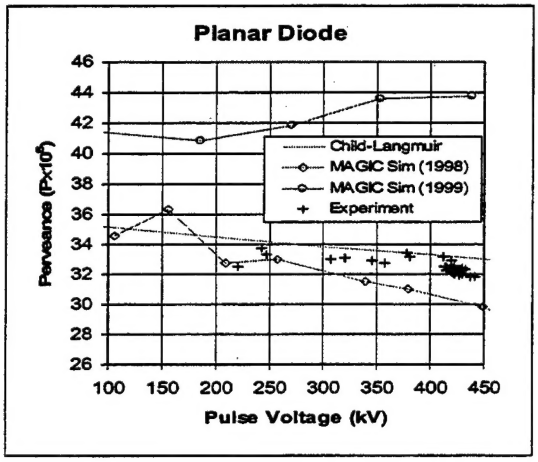

Figure 2: Planar diode perveance.

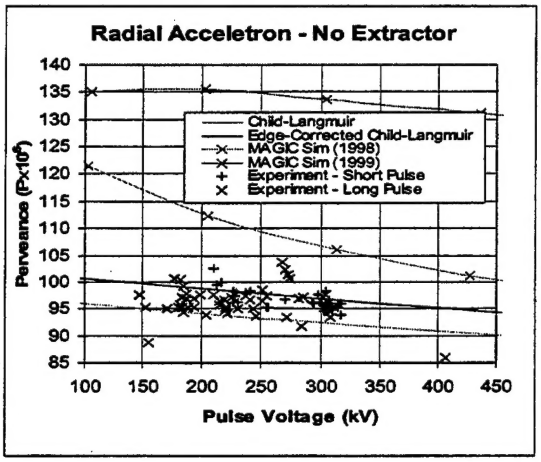

Figure 3(a): Radial acceletron perveance (no extractor).

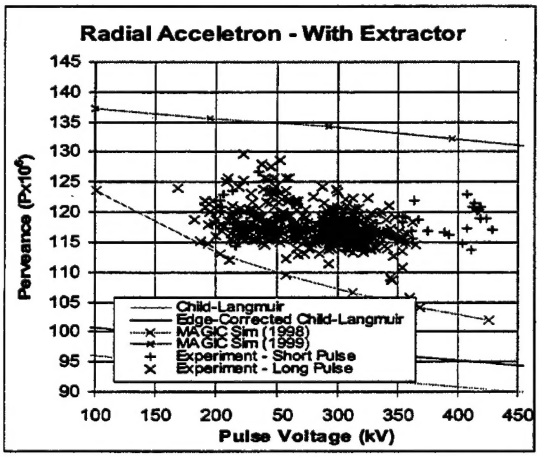

Figure 3(b): Radial acceletron perveance (with extractor).

No measurable RF was noted for any extractor plate separation (7.0 cm $\leq$ d $\leq$ 10.0 cm) or any achievable shot voltage (203 kV $\leq$ V $\leq$ 429 kV). The minimum measurable signal (10 mV from a zero-area B-dot probe) corresponds to an RF output power of approximately 42 kW at 3.2 GHz. The peak input power (403 kV shot voltage) was approximately 11 GW.

Small amounts of RF were noted in both the 3 GHz and 6 GHz bandpass filters for extractor plate separations of 8.0 cm and 8.5 cm; no measurable RF was noted at other plate separations. The minimum measurable signal corresponds to approximately 230 W RF power at 3.2 GHz. In the 3 GHz filter, the measured dB/dt values of 1.0×10^6 $^T/_{sec}$ at 8.0 cm separation and 5.5×10^6 $^T/_{sec}$ at 8.5 cm separation correspond to output powers of 54 KW and 1.6 MW respectively. Post-experiment re-calibration of the Blumlein voltage sensor gave maximum shot voltages for this series of approximately 320 kV - about the voltage at which simulation indicated measurable RF would first be produced.

Significant amounts of RF were noted in both the 3 GHz and 6 GHz bandpass filters for extractor plate separations of 8.0 cm and 8.5 cm; no measurable RF was noted at other plate separations. The minimum measurable signal corresponds to approximately 230 W RF power at 3.2 GHz. In the 3 GHz filter, the measured dB/dt values of 6.3×10^6 $^T/_{sec}$ at 8.0 cm separation and 3.1×10^7 $^T/_{sec}$ at 8.5 cm separation correspond to output powers of 2.1 MW and 52 MW respectively. The corresponding MAGIC simulation predictions were B-dot values of $3 * 10^6$ $^T/_{sec}$ and 8×10^7 $^T/_{sec}$ respectively. Post-experiment re-calibration of the Blumlein voltage sensor gave maximum shot voltages for this series of approximately 365 kV - about the voltage at which simulation indicated strong RF would be produced.

Overall, the experimentally measured prototype operating characteristics and the values predicted by simulation and 1-D analysis compared poorly. The large physical size and multiple connected (coupled) cavities result in a plethora of near-degenerate RF modes. The major limitation of the 1-D analysis is that all the free energy available from the nonlinear diode voltage-current relationship is assumed to go into a single RF mode. In reality, the free energy will be distributed across all the modes that grow. For the prototype radial acceletron, the large number of RF modes that satisfy the requirements for RF growth means that the 1-D analysis will over-predict RF growth rates for any single mode. The large difference in size between key physical elements of the prototype is a significant departure from the fundamental requirements of the numerical algorithms used in the PIC simulation. The small grid sizes required in the *A-K* gap region and at the entry to the extractor transmission line, combined with the large physical size of the cavities, results in either grid cells with large aspect ratios or too many cells for the available computer memory. Even with sufficient computational memory, the small grid dimensions require a small time step to maintain numerical stability. However, this small time step results in such a large number of steps required to solve the problem that accumulation of numerical errors becomes significant. To obtain reasonable correspondence between analysis, simulation and experiment, the prototype should be re-designed to avoid the limitations inherent in the available predictive methods.

In summary, the RF generation efficiency for a device based on the radial acceletron design will be low; the theoretical maximum efficiency of 0.39 occurs at zero initial RF growth, and if a reasonable value of device-to-radiation impedance ratio of $18\Omega/50\Omega$ is assumed, the maximum efficiency is only 0.09. Note that this is an efficiency of RF generation of all RF, across all the frequency regions where RF growth is possible. The efficiency of any single RF lie will be reduced by the amount of energy used for growth of unwanted frequencies.

B. Techniques to Achieve Greater Output Power from HPM Sources

The tasks that we worked on in this section can be summarized with the heading used above. In last year's annual report we provided details which we summarize here.[1]

High Power Microwave source research has been ongoing since the late 1960's. The pioneers in this field have included John Nation and his group at Cornell University [6] and Nikolay Kovalev and his colleagues at the Institute of Applied Physics, Nizhny Novgorod (formerly Gorky) [7]. These early HPM sources evolved directly because of the innovation of modern pulsed power [8]. Pulsed power provides the capability of generating intense relativistic (high perveance) electron beams.

The HPM community experienced the "power derby" (see page 398 in the book by Benford and Swegle [9]) from the late 1970's through the early 1990's. During this period researchers were competing to develop sources and configurations that could outperform earlier achievements. Although many of the results reported in the literature during this period likely have large error bars associated with the measurements (attributable to many factors), the overall trend of radiated power increasing during this time period is credible. The optimism of this period is reflected in Table 12.2 of [9], which seeks to predict future directions in HPM. Radiated peak power levels of 100 GW and radiated energy exceeding 10 kJ/pulse were expected to have been achieved by now.

A sobering realization occurred in the 1990's as radiated powers in the range of 1-10 GW were achieved, and energies per pulse on the order of 1 kJ were documented. These parameters were achieved through considerable effort, and through the added benefit of sophisticated three-dimensional computational modeling tools that were not available before (see Chapter 11 of [10]). Unfortunately, these parameters seem to have become fixed. The term "pulse shortening" came into vogue (see Chapter 4 of [11]) and encompassed the various causes for the concomitant decrease in pulse length as peak powers increased (radiated energy staying constant). This has led to a reassessment of the way the HPM community has been developing its sources, and has manifested in a significant decline in research on new source configurations. Much of the focus has been on improving the vacuum environment of the sources; developing cathodes that can yield minimal plasma, yet deliver the requisite electron current densities at low electric fields; and invoking better design to ensure that the intense electron beam impacts as little of the electrodynamic structure as possible as it gives up its kinetic energy and passes towards the collector.

Figure 4 depicts a block diagram of an HPM system. The HPM source itself comprises the electron beam source, t he beam-to-rf convertor (the electrodynamic structure), and the rf extractor. Components are then added to the extractor region to facilitate radiation through the use of an appropriate antenna. This block diagram basically follows the traditional thinking of HPM sources. Each of the components is viewed as a separate and discrete element, and the final HPM system is simply the "connection" of the various discrete

[1] This section of the report is adapted from an invited talk presented by the PI of this grant at the *2002 Power Modulator Symposium and High Voltage Workshop.*

elements. In our view, in order to see a resurgence of a "power derby" in HPM, it is necessary to abandon this view in favor of an approach that considers an HPM source as one integrated continuum, designed from electron gun to collector to optimize its performance.

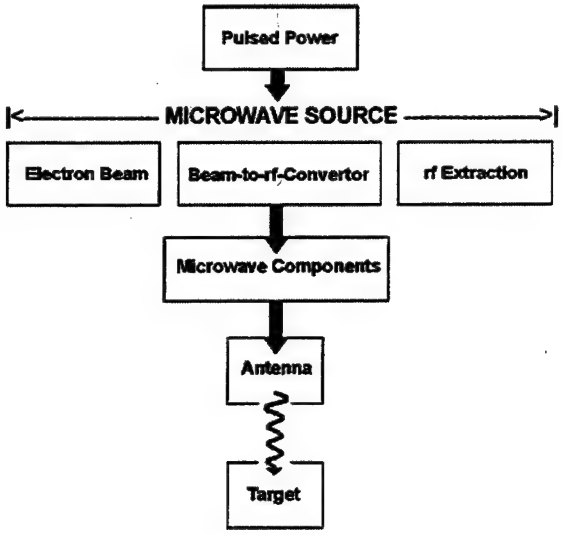

Figure 4. A block diagram depicting an HPM system. Pulsed power is used to energize the electron beam diode. The microwave source itself comprises the electron beam, the beam-to-rf convertor (typically termed the interaction space), and the rf extractor. Once rf is extracted from the interaction space, components are used to couple the rf to an antenna, which ultimately radiates the energy towards some target (figure from [11]).

In addition, as part of this "rethinking," one should recognize that pulse shortening is a problem that will exist as peak power levels increase. Certainly improved vacuum environment and cleaning protocols will be necessary, but the reality is that a successful approach to increasing radiated powers will have to involve decreasing the electric field stresses inside the electrodynamic structures. This implies operating with larger diameter systems that introduces the complication of an overmoded structure. However, clever techniques of mode selection will be the key to managing this complication.

We not present a list of HPM sources that represent this rethinking.

Relativistic Magnetron with Diffraction Output

Relativistic magnetrons of the traditional design (as, for example, the A6 magnetron [10]) are loads with impedance that typically exceed 100 Ω (Fig. 5). Although increasing the radiation power by increasing the beam current is always preferable to using higher voltages, this has not been invoked in relativistic magnetrons. The main obstacle is the small dimension of the interaction space in microwave sources that is limited by the requirement of single mode operation. For some applications, a low impedance microwave source is desirable. As an example, we may consider applications that would be based on compact high power sources of microwaves that are powered using magnetocumulative generators (MCG's). In order to

transfer energy from such a high current generator to a load with high impedance, great effort is required to implement a suitable impedance matching network.

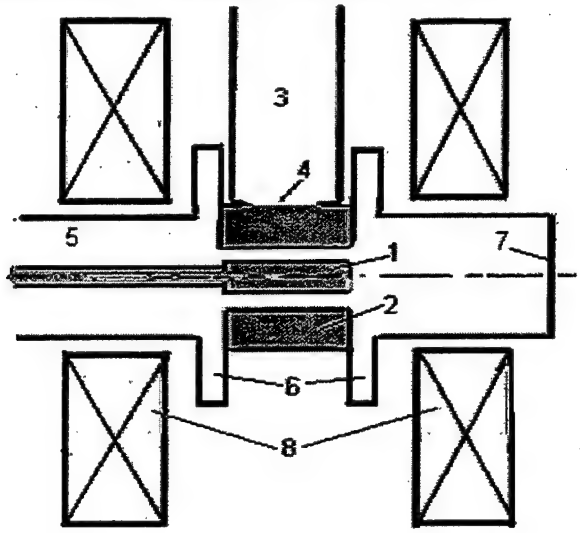

Figure 5. Schematic of a traditional design of a relativistic magnetron: (1) - explosive emission cold cathode; (2) - resonant system; (3) - output waveguide; (4) - iris; (5) - coaxial line; (6) - side cavities; (7) - electron dump; (8) – Helmholtz coils.

In contrast, consider a relativistic magnetron with diffraction antenna output that could operate with very high current (Figs. 6 and 7). The advantages of the magnetron with diffraction antenna in comparison to traditional relativistic magnetrons are many and are summarized below in Table 1 [12].

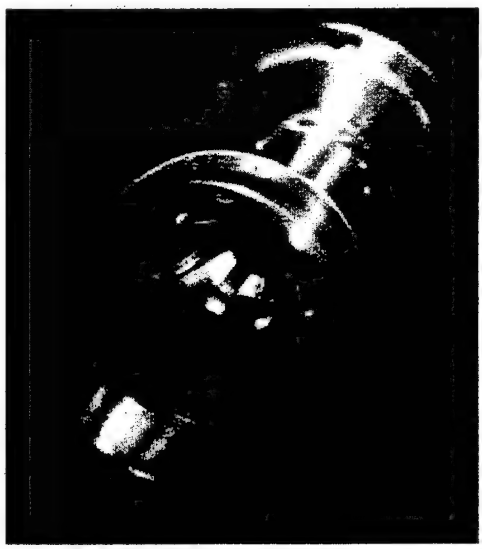

Figure 6. Photograph of an X-band relativistic magnetron with diffraction radiation output.

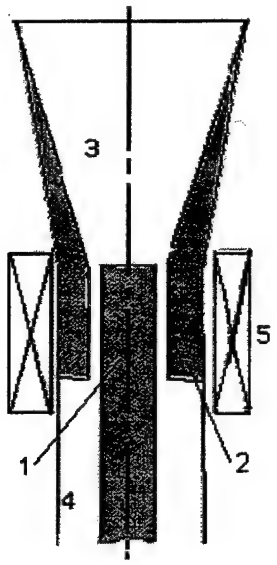

Figure 7. Schematic drawing of an X-band relativistic magnetron with diffraction radiation output. (1) - cathode; (2) - resonant system; (3) - horn antenna; (4) - coaxial line; (5) - solenoid.

Table 1. Advantages of relativistic magnetron with diffraction output.

i.	High resistance to microwave breakdown.
ii.	Absence of dangerous transitions to unloaded types of oscillations that allow one to increase the number of resonators up to the limit determined by the overlapping of the synchronism bands; this implies that any mode can be used for operation.
iii.	The selection of longitudinal modes is independent of the axial length of the magnetron; the length can be chosen based only on the required amplitude of the microwave field.
iv.	The volume of magnetic field required is small.
v.	The radiation pattern can be transformed directly within the diffraction antenna
vi.	Capability to operate with extremely high current (as a low impedance load of a high voltage pulser) because of the possibility of enlarging the interaction space and the arbitrary choice of the magnetron's axial length.

Recall that extremely large radiated powers $P \approx 10$ GW in an L-band magnetron [13] with a small volume of the interaction space $V < \lambda^3$ (λ is the operating wavelength) were demonstrated in the first experiments more than 20 years ago. These power levels have yet to be exceeded by other magnetrons.

The configuration shown in Figs. 6 and 7 embody the "rethinking" discussed earlier. By viewing Fig. 6, one can see that the cathode is integrated with the electrodynamic structure as is the case in traditional magnetron. In addition, however, the output antenna is a continuum

that comprises the magnetron vanes. Furthermore, the mode convertor and beam collector are integrated within the antenna configuration as well. As a result, one can see that you cannot separate this HPM source into its discrete elements. A final advantage of this configuration is that the spent current drifting axially away from the cavity enters an increasingly larger diameter section, thereby naturally limiting the loss current through virtual cathode formation.

Complete details concerning this source can be found in [12].

Hybrid Antenna-Amplifier

Another example of an HPM source that embodies "rethinking" is the hybrid antenna-amplifier indicated in Fig. 8.

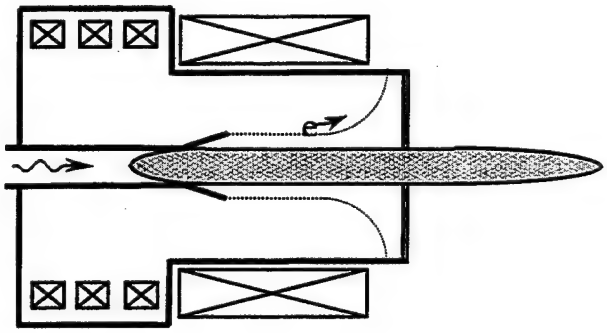

Figure 8. Example of a hybrid antenna-amplifier. A linear induction accelerator is shown driving an annular electron beam propagating outside a dielectric rod. The antenna feed signal serves as the TWT rf drive.

A traveling wave tube can be combined with a surface wave antenna if a relativistic electron beam propagates along the antenna slow wave structure. In such a hybrid antenna-amplifier device, the TWT rf drive would simultaneously serve as the antenna feed signal. In the cylindrical geometry of the hybrid antenna-amplifier, an annular beam propagates outside a rod antenna, and the operating mode is the fundamental non-axisymmetric HE_{11} mode. The salient features of this concept for a high-power microwave source are discussed in [14], including the effects of nonlinear multi-mode considerations. This device concept has yet to be studied experimentally, but nevertheless suggests that one might obtain interesting parameters through the integration of the electrodynamic interaction with a radiating antenna.

As mentioned earlier, achieving another order of magnitude increase in output power will likely involve operation with large diameter, overmoded structures. Managing mode competition will be critical to successful operation of these devices.

A widespread method to provide spatial coherence of output radiation in relativistic generators is the application of selective feedback through the use of Bragg reflectors placed at each end of an oversized electrodynamic system [15-21]. To achieve selective feedback

while not interfering with the electron beam in different types of resonant traveling wave tubes such as Cherenkov generators, ubitrons, or free electron lasers, Bragg reflectors made from cylindrical periodically corrugated waveguides are used. The dependence of the periodic profiles of the Bragg reflectors on the azimuthal coordinate θ and axial coordinate z is arbitrary; as an example, it can be a sinusoidal corrugation described by

$$R(\theta,z) = R_0 + l_0 \cos(\overline{m}\theta + \overline{h}z), \tag{1}$$

which is the most common one in use. Here $|\overline{h}| = 2\pi/d$ is a constant of the periodic system (the Bragg reflector), R_0, l_0, and d are the average radius, amplitude, and period of corrugation, respectively. The Bragg reflectors can be helical corrugations with a number of $\overline{m}$ spirals, or an axially symmetric corrugation ($\overline{m} = 0$). Such reflectors transform a rotating forward wave with azimuthal index m_1 and propagation constant h_1 to a rotating backward wave, propagating in opposite direction with azimuthal index

$$m_2 = m_1 \pm \overline{m} \tag{2}$$

and longitudinal wave number

$$h_2 = \overline{h} - h_1. \tag{3}$$

The application of two such Bragg reflectors at the ends of a waveguide (Fig. 9) allows one to separate the operating two-mode solitary structure of the electromagnetic field, *i.e.,* to achieve the ability to select the frequencies and types of waves.

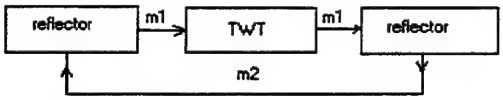

Figure 9. Block diagram of a microwave generator using single channel feedback to achieve mode selection in an overmoded system.

This method of mode selection can lead to significant progress in the increase of energetic parameters of microwave oscillators. Above all, for provision of selective feedback there is the possibility of using backward wave amplifiers operating in the regenerative regime of amplification. Application of such non-linear reflectors, in which the reflection coefficient depends on the incident signal, allows us to operate in the regime of generation with self-modulation, which enables us to provide a short transit time and operation with high efficiency, among other salient features.

To summarize this section of the report, in order for high power microwave sources to radiate power levels that exceed present accomplishments by an order of magnitude and greater will require to view these systems as integrated devices, no longer separating them into discrete, constituent components. Furthermore, in order to avoid pulse shortening, devices whose electrodynamic structures are multimoded will inevitably be required. This issue will have to be managed using clever techniques.

C. HPM Generation in a BWO using a Hollow Beam Generated from a Disk Cathode

For the first time, a new disk cathode has been incorporated into the design of a BWO in an effort to lengthen the microwave pulse (Fig. 10). The basic principle for pulse lengthening was to minimize the dense plasma that forms on an explosive emission cathode. The motivation for this approach in UNM's BWO was based upon past research which revealed that this dense plasma, which was formed on a graphite "cookie-cutter" cathode, caused the electron beam to expand radially and thus intercept with the cutoff neck upon entering the SWS. The consequence of this action was an impedance collapse in the A-K gap. As Loza *et al.* [22], had shown, the plasma that forms on a disk cathode is as little as the tip of the disk. Using basic plasma pressure arguments, they showed that this plasma tends to migrate along the magnetic field lines rather than expand radially. A radially expanding plasma leads to an expanding electron beam which was observed in the "cookie-cutter" case.

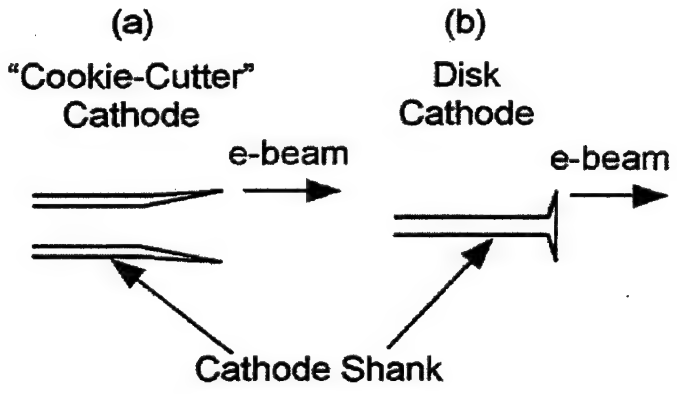

Figure 10. Cross-sections of the (a) "cookie-cutter" cathode (also known as knife-edge cathode) and (b) the disk cathode (also known as a "pizza-slicer" cathode).

Beam intercepting targets placed in the middle of the SWS without microwaves present indicated that the electron beam expanded to meet the dimensions of the cutoff neck for the "cookie-cutter" cathode, while the disk cathode maintained a more stable cross section which was smaller than the cutoff neck opening. While these diagnostics were not taken in the presence of microwaves, they do indicate that the disk cathode produced a more stable beam. Of course, with microwaves present, beam disruptions occur due to the intense rf fields generated in the SWS. Previous measurements in UNM's BWO showed that the beam breaks up after about 100 ns in the presence of microwaves. These measurements were not taken for the disk cathode; however, it was hypothesized that the more stable beam would hold off this beam breakup behavior for a longer period of time.

Initial results with a 20 mm stainless steel disk cathode proved to be extremely promising as the microwave pulselength and power was nearly doubled as compared to all previous studies with a 20 mm graphite "cookie-cutter" cathode. Results for the 20 mm stainless steel "cookie-cutter" cathode yielded similar (and sometimes better) results as compared to the 20 mm stainless steel disk cathode. Although the stainless steel material was used, the electron current was still increasing as the voltage dropped.

To improve the beam current characteristics, a copper insert was installed in an effort to provide a better magnetic field geometry which was crucial especially for the disk cathode operation. This modification led to increased compression of the beam. The beam was then compressed too much so that it did not couple efficiently within the SWS to provide much microwave interaction. The diameter of each cathode geometry was then increased to 23 mm. Beam targets were again used to determine the cross sections of each beam without microwaves present. This diameter produced beam cross sections that were similar to the ones for the 20 mm cathodes. Also, since the beam diameter was increased, the current should increase. The A-K gap was increased from 2.5 cm to 3.5 cm to reduce the current to similar values as with the 20 mm cathodes.

The data from the experiments revealed that the stainless steel versions of the "cookie-cutter" and the disk cathode produced pulsewidths of about 150 ns with about 50-60 MW output power. A crude analysis of the half power pulse widths (FWHM pulsewidths) identified the disk cathode as the better cathode (see Tables 2-3).

The results obtained experimentally suggest that using stainless steel instead of graphite as a cathode material had the biggest effect in lengthening the microwave pulse. Clearly, there are many issues contributing to the still present pulse shortening in the BWO at UNM. Simply changing one parameter does not mean that other parameters can remain the same.

Table 2. Initial experimental measurements with 23 mm stainless steel "cookie-cutter" and disk cathodes.

Input Parameters:	*"Cookie-cutter"* **Pulselength and** *Power*	*Disk* **Pulselength and** *Power*
Cathode Voltage: 400 kV **Beam Current:** 1-2 kA	40-55 ns 15-25 MW	80-100 ns 30-45 MW
Cathode Voltage: 425kV **Beam Current:** 1.5-2.5 kA	80-100 ns 35-45 MW	100-125 ns 30-45 MW
Cathode Voltage: 475 kV **Beam Current:** 1.5-3 kA	140-150 ns 40-50 MW	140-160 ns 45-60 MW
Cathode Voltage: 500 kV **Beam Current:** 1.5-3 kA	140-150 ns 45-55 MW	140-160 ns 45-60 MW

Table 3. FWHM microwave pulsewidths for the 23 mm disk and "cookie-cutter" cathodes.

Input Parameters:	"Cookie-cutter" *FWHM pulsewidth*	**Disk** *FWHM pulsewidth*
400 kV	~35 ns	? (too many oscillations)
475 kV	~50 ns	~70 ns
500 kV	~50 ns	~ 85 ns

Beam Current Limitation Revisted

One of the most important consequences of the research presented here is the analysis of the Fedosov limiting current [23] versus the space charge limiting current. The derivation of the Fedosov current is based on the initial conditions present on a coaxial cathode that would be valid for the "cookie-cutter" geometry. The electric field solution in the derivation is the same as the solution for a simple coaxial capacitor. On the other hand, the disk cathode is solid and thus the potential is constant on the surface. Although the current emitted from the disk cathode is nearly the same geometry as the "cookie-cutter" cathode, the Fedosov solution should be invalid. Instead, the disk cathode can maintain a higher current up to the space charge limiting value. This consequence has important ramifications for the output power in beam–driven devices. The operating voltage is essentially a characteristic of the pulsed-power apparatus. The injected current is a function the A-K gap characteristics, such as cathode dimensions, drift tube dimension, geometry, and A-K gap distance. The "cookie-cutter" cathode's current is Fedosov limited to a value that is less than the space charge limit. The disk cathode current can support the space charge current limit and hence inject more current. More current leads to more power. This is perhaps why the disk cathode exhibited slightly higher power levels than the "cookie-cutter" case. For an operating voltage of 500 kV, the space charge limiting current is about 3.9 kA versus the Fedosov current of 2.9 kA. This represents a 25% increase at this operating voltage. At higher voltages, the increase would be greater and lead to more efficiency in these devices. From the experimental results at the higher voltages (~500 kV), the disk was better than the "cookie-cutter" cathode when comparing the FWHM pulsewidths. However, the disk cathode's microwave power was slightly higher than the "cookie-cutter" cathode, but not as high as 25%. The calculation of the beam currents for the space charge limited versus the Fedosov limited cases assumes very ideal conditions and that the beam is traversing a smooth walled waveguide. In the BWO, the spacing and geometry of the A-K gap play an important part in the beam current calculations. Numerical techniques should be used to investigate this current limit.

This result is not absolutely consistent with the experimentally obtained results. The disk cathode did outperform the "cookie-cutter" cathode; however, at higher voltages (~500 kV) the experimental results (regarding microwave power and pulse duration) from each seem to be converging to the same values regarding pulse length and power (see Table 2). For the operating regime of UNM's BWO (400-500 kV), the space charge current exceeds the Fedosov current by 20-25%. At higher voltages the space charge current remains about 30% greater than the Fedosov current. The beam current measurements for each type of cathode were compared. The currents seemed to be nearly identical; however, the poor calibration as well as oscillations present within the signals (Fig. 11) made this interpretation erroneous. Other factors are playing a role here that may or may not have to do with beam stability. The basic construction of the BWO is the most fundamental issue in increasing the pulse width and investigating pulse-shortening effects. Many of the current design flaws will be addressed when an upgraded BWO is built at UNM in the near future, utilizing a brazed ceramic insulator stack that was acquired from Titan/PSD from an earlier DURIP grant.

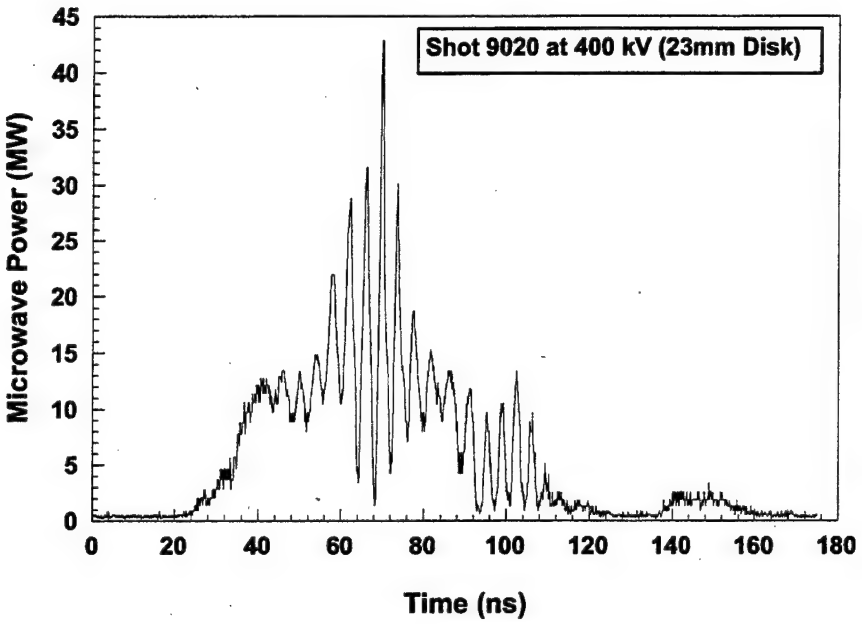

Figure 11. Microwave output power for a 23 mm stainless steel disk cathode at 400 kV peak voltage. Many oscillations were evident on shots at this low voltage, attributed to virtual cathode effects since the beam current exceed the Fedosov current [24].

Communication with an HPM-Driven Interplanetary Sail

Microwave-propelled sails were first introduced by the late Robert Forward as a continuation of his laser-driven sail concept [25,26]. Missions beyond our solar system are impossible using present chemical propellant-based propulsion systems because the weight of the necessary fuel would be prohibitively excessive. The high power microwave-driven sail is man's only alternative to nuclear-fueled spacecraft for deep-space missions. Microwave-driven sails have the advantage that energy is expended to accelerate only the sail with its payload, not the propelling beam generator [27]. Interstellar flight requires speeds >>100 km/s. Of particular interest for scientists would be a mission to the region known as the Oort Cloud, composed of thousands of millions of comets extending beyond the Sun for a light year and beyond. Microwave-propelled sails are accelerated using beamed microwaves and although electromagnetic waves (photons) have no mass, they do have both axial and angular momentum components. A reflected beam of light exerts a force F proportional to its power P via $F = 2P/c$ where c is the speed of light (3×10^8 m/s).

A severe limitation to beamed microwave-driven sails is finding a material that can accommodate the severe mission constraints. The invention of ultralight, strong, and high-temperature-compatible carbon material has made microwave-propelled sails a serious contender because carbon does not melt; it sublimes at very high temperature [28]. Extremely high temperatures are needed because acceleration is strongly temperature limited, as is evident from the following consideration. The acceleration a from photon momentum produced by a power P on a thin film of mass m and area A is [29]

$$a = [\eta + 1]\frac{P}{MA}c \tag{4}$$

where η is the reflection of the film of absorbtivity[1] α and M is the mass per unit area. Carbon fiber sail material with ~1% transmissivity[1] can be produced. Thus, αP will be absorbed from the incident power on the film. This absorbed power must be radiated away from both sides of the film which may be at different temperatures. We describe this power with an average temperature T and emissivity[2] ε by the Stefan-Boltzmann law

$$\alpha P = 2A\varepsilon\sigma T^4 \tag{5}$$

where σ is the Stefan-Boltzmann constant (5.67×10^{-8} W/m^2-K^4). If we eliminate P and A, the sail acceleration is given by

$$a = \left(\frac{2\sigma}{c}\right)\left[\varepsilon\frac{(\eta+1)}{\alpha}\right]\left(\frac{T^4}{M}\right). \tag{6}$$

Clearly the acceleration is strongly temperature-dependent. All materials tested in early studies (Al, Be, Nb, *etc.*) could not be used for liftoff from Earth since their melting temperature limited the achievable acceleration.

There are similarities between microwave-propelled sails and interplanetary missions. The channels in both cases are free-space (except for transmission through the ionosphere and atmosphere) with almost no noise (unless we account for flares), the distance traversed is very large, and ultra sensitive receivers are needed to extract the received signal.

Missions beyond the solar system have been successfully accomplished by Voyager 1 and 2. Voyager 1 is now the most distant man-made object in the universe, was at a distance of 12 billion kilometers (80 Astronomical Units (AU)) (1 AU = 1.5×10^{11} m) from the sun as of January 2001, while Voyager 2 was at 9.4 billion kilometers (62.7 AU) from the sun as of January 2001. Voyager 1 is escaping from the solar system at a speed of about 3.6 AU per year (~17.1 km/s), 35 degrees out of the ecliptic plan to the north. Voyager 2 is also escaping from the solar system at a speed of about 3.3 AU per year (~15.7 km/s), 48 degrees out of the ecliptic plan to the south.

Since the distance from a sail to the Earth is presumably large, by the time the signal arrives on Earth its power decreases considerably so that we need ultra sensitive receivers both on Earth and on the spacecraft (or the sail). The Deep-Space Network's (DSN's) receivers are sufficiently sensitive to receive signals of power –127.4 dBm or 10^{-16} W (Voyager 2's uplink received power) and –145.5 dBm or 10^{-18} W (Voyager 2's downlink received power) [30]. In our simulations, we showed that we can receive powers of 10^{-13} or 10^{-14} W (depending on the transmitter power and the distance). The transmitted power of Voyager 2 is 72.6 dBm or 18 kW for the uplink and 40.9 dBm or 12.3 W for the downlink, while the 70-meter-antenna at the Goldstone Communication Complex is capable of transmitting a maximum of 400 kW. The microwave-propelled sail communication system we proposed has greater coding gain

[2] Absorbtivity is the ratio of absorbed power to incident power, transmissivity is the ratio of transmitted power to incident power, and emissivity is the ratio of emitted power to power emitted from a blackbody.

than the Voyager mission because we are using Turbo codes.

Encoding/decoding is very important because coding gain compensates for the very weak received signal power levels. The Voyagers' telemetry link also suffers from the noise in the communication channel as do other deep-space links, causing bit errors. The rate of errors is reduced by error-correcting codes. Such codes increase the redundancy of the signal by increasing the number of bits transmitted relative to the information bit rate. The Golay encoding algorithm used at the Jupiter and Saturn phase of the mission required the transmission of one overhead bit for every information bit transmitted (100% overhead). Voyager had an experimental Reed-Solomon data encoder, expressly developed for the greater communication range of the Uranus and Neptune phase of the mission. The new Reed-Solomon encoding scheme reduced the overhead to about one bit in five (20% overhead) and reduced the bit error rate in the output information from 5×10^{-3} to 10^{-6} [31]. In our simulations we used Turbo codes that provide performance close to the Shannon Limit [32]. The coding gain of Turbo codes is greater than traditional cyclic block codes and convolutional codes.

The DSN is able to transmit signals at L-Band, S-Band, X-Band, and Ka-Band and receive at S-Band and X-Band. Voyagers use S-Band for uplink and S-Band and X-Band for downlink. Also, for the future missions, DSN is planning to use Ka-Band for both the uplink and downlink. We selected X-Band for both uplink and downlink for the microwave-propelled sail system simulations.

The results of our simulations were that we had an acceptable received power level for the scale distance of 1 AU. However, when we scaled the channel to the distance of the Oort Cloud (10^4 AU's), we see that the DSN's ultra sensitive receivers are not able to receive those power levels since they are much less than the minimum acceptable levels. We calculated the maximum distance between the sail and the Earth for successful communications as 271.40 AU's. Clearly additional development in technology would be required.

Future work will entail scaling this proposed channel to even greater distances. In so doing, the time delay of the signal inevitably becomes a factor to be included. For travel to distances as far as the Oort Cloud, more efficient codes should be developed and higher transmitter powers will be required.

Complete simulation results can be found in [33].

REFERENCES

1. W. Hansen, *et al.,* "High Frequency Radio Apparatus," U.S. Patent 2,259,690; 21 Oct 1941.
2. M.J. Arman, "High Power Radial Klystron Oscillator," *Proceedings SPIE,* vol. 2557, 21, 1995.
3. M.J. Arman, "Radial Acceletron, a New Low-impedance HPM Source," IEEE Trans. Plasma Sci., vol. 24, 964, 1996.
4. B. Goplen, *et al., MAGIC User's Manual MRC/WDC-R-409* (Mission Research Corp., Newington, VA, 2000).
5. R.L. Wright, *Evaluation of a Prototype Radially-Symmetric Transit-Time Oscillator Using Simulation and Experiment,* Ph.D. Dissertation, University of New Mexico (Albuquerque, NM 2002).
6. J.A. Nation, "On the Coupling of a High-current Relativistic Electron Beam to a Slow Wave Structure," Appl. Phys. Lett., vol. 17, p. 491, 1970.
7. N.F. Kovalev, M.I. Petelin, M.D. Raiser, A.V. Smorgonsky, and L.E. Tsopp, "Generation of Powerful Electromagnetic Radiation Pulses by a Beam of Relativistic Electrons," Pis'ma Zh. Eksp. Teor. Fiz., vol. 18, p. 232, 1973 (JETP Lett., vol. 18, p. 138, 1973).
8. Modern pulsed power refers to the activities attributed to the late Charlie Martin and his colleagues at AWRE in Aldermaston, England in the 1960's. See T.H. Martin, A.H. Guenther, and M. Kristiansen, Eds., *J.C. Martin on Pulsed Power* (Plenum Press, New York, NY, 1996).
9. J. Benford and J. Swegle, *High-Power Microwaves* (Artech House, Norwood, MA, 1992).
10. R.J. Barker and E. Schamiloglu, Eds., *High power Microwave Sources and Technologies* (IEEE Press, Piscataway, NJ, 2001).
11. G. Bekefi and J. Orzhechowski, "Giant Microwave Bursts Beam Magnetron," Phys. Rev. Lett., vol. 37, p. 379, 1976.
12. M. Fuks and E. Schamiloglu, "Optimization of the Parameters of a Relativistic Magnetron with Diffraction Output," Proceedings SPIE Intense Microwave Pulses IX, April 2-3, 2002, Orlando, FL, p. 18.
13. V.E. Nechaev, M.I. Petelin, and M.I. Fuks, "Prospects of Magnetron Devices with Relativistic Electrons," Pis`ma v ZhTF (in Russian), vol. 3, p. 763, 1977.
14. A.S. Shlapakovski, I.I. Grushin, Z. Zhou, and E. Schamiloglu, "Drive' Signal Frequency Multiplication in a Hybrid Antenna-Amplifier Device," Proceedings 13th IEEE International Pulsed Power Conference, Las Vegas, NV, June 2001, p. 553.
15. E.B. Abubakirov, M.I. Fuks, and N.F. Kovalev, "High-selectivity Resonator for Powerful Microwave Sources," Proceedings of International Conference "Beams`96," Prague, Czech Republic, vol. 1, p. 410, 1996.
16. E.B. Abubakirov, M.I. Fuks, and N.F. Kovalev, "Relativistic TWT with Multi-channel Non-linear Feedback," Papers of International Workshop on High Power Microwave Generation and Pulse Shortening, Edinburgh, P3-10, 1997.
17. G.G. Denisov, M.G. Reznikov, "Corrugated Circular Resonators for Microwave Relativistic Oscillators," Izv. VUZov, Radiofizika (Russian), vol. 25, p. 562, 1982.
18. V.L. Bratman, G.G. Denisov, N.S. Ginzburg, and M.I. Petelin, "FEL`s with Bragg

Reflection Resonators," IEEE J. Quantum Electron., vol. 19, p. 282, 1983.
19. T.J. Orzechowski *et al.*, "High-efficiency Extraction of Microwave Radiation from a apered-wiggler Free Electron Laser," Phys. Rev. Lett., vol. 57, p. 2172, 1986.
20. E.B. Abubakirov, M.I. Fuks, V.A. Gintsburg *et al.*, "Cherenkov Relativistic Oscillators of Coherent Electromagnetic Radiation with Multimode Sectioned Electrodynamic Systems," Proceedings of International Conference "Beams`90," vol. 2, p.1105, 1991.
21. M.I. Fuks and N.F. Kovalev, "Selective Multi-Channel Feedback," IEEE Trans. Plasma Sci., vol. 30, pp. 1147-1150 (2002).
22. O.T. Loza and P.S. Strelkov, "Generation of an Annular REB of Microsecond Pulse Duration and Stabilized Transverse Dimension in a Diode with a Field-Emission Cathode," Proceedings 12th International conference on High Power Particle Beams (Haifa, Israel, 1998), p. 357.
23. A.I. Fedosov, E.A. Litvinov, S. Ya. Belomytsev, and S.P. Bugaev, "Characteristics of Eletron Beams in Diodes with Magnetic Insulation," Translated from Izvestiya Vysshikh Uchebnykh Zavedenii, Fizika, No. 10, pp. 134-135, 1977.
24. K.D. Hahn, *Operation of a Long-Pulse Backward Wave Oscillator Utilizing a Disk Cathode*, Ph.D. Dissertation, University of New Mexico (Albuquerque, NM, 2002).
25. R.L. Forward, "Roundtrip Interstellar Travel Using Laser-Pushed Light Sails," *J. Spacecraft*, pp. 21, 187, 1984; R.L. Forward, "Starwisp: An Ultra-Light Interstellar Probe," *J. Spacecraft*, pp. 22, 345, 1985.
26. See, also, *Beamed Energy Propulsion, Proceedings First International Symposium on Beamed Energy Propulsion, AIP Conference Proceedings 664,* A.V. Pakhomov, Ed. Melville, NY: AIP, 2003.
27. J. Benford, "Flight and Spin of Microwave-Driven Sails: First Experiments," Microwave Sciences Inc., Lafayette, CA, 2001.
28. Material invented and manufactured by Energy Science Laboratories, Inc., www.esli.com.
29. J. Benford, G. Benford, K. Goodfellow, R. Perez, H. Harris, and T. Knowles, "Microwave Beam-Driven Sail Flight Experiments," *in STAIF 2001 Conference*, University of New Mexico, Albuquerque, NM, 2001.
30. http://voyager.jpl.nasa.gov/mission/interstellar.html.
31. R. Ludwig and J. Taylor, *DESCANSO Design and Performance Summary Series, Article 4, Voyager Telecommunications*. Jet Propulsion Laboratory, California Institute of Technology, Pasadena, California, 2002.
32. C.E. Shannon, "A Mathematical Theory of Communication," *Bell System Technical Journal,* vol. 27, pp. 379-423 and 623-656, 1948.
33. I.S. Bakim, C.T. Abdallah, and E. Schamiloglu, "Communicating with Microwave-Propelled Sails," accepted for publication in IEEE Antennas and Propagation Magazine (2003).

PERSONNEL

EECE Faculty
Dr. Edl Schamiloglu (consortium PI), Professor
Dr. Chaouki Abdallah (UNM Co-PI), Professor

EECE Research Faculty
Dr. Mikhail Fuks (0.5 FTE)
Dr. Nikolay Kovalev (Visiting professor, 2 months)

Graduate Students

Robert Wright – Ph.D. – *Evaluation of a Prototype Radially-Symmetric Transit-Time Oscillator Using Simulation and Experiment* (December 2003) (conference travel supported by New World Vistas)

I. Sezi Bakim – M.S. - *Communication System Design for a Microwave-Propelled Sail* (May 2003)

PUBLICATIONS

1. Journal Papers

a) A.S. Shlapakovskii, E. Schamiloglu, and I.I. Grushin, "Multiplication Of The Drive Signal Frequency In A Relativistic Microwave Amplifier With A Rod Slow-Wave Structure," Technical Physics, vol. 47, pp. 1434-1439 (2002).

b) N.F. Kovalev, S.V. Fil'chenkov, M.I. Fuks, and E. Schamiloglu, "Axisymmetric Waves in Dielectric Corrugated Rods and Systems of Periodic Dielectric Rings," IEEE Trans. Plasma Sci., vol. 30, pp. 1082-1088 (2002).

c) E.B. Abubakirov, A.N. Denisenko, M.I. Fuks, N.G. Kolganov, M.I. Petelin, A.V. Savelyev, E. Schamiloglu, E.I. Soluyanov, and V.V. Yastrebov, "An X-Band Gigawatt Amplifier," IEEE Trans. Plasma Sci., vol. 30, pp. 1041-1051 (2002).

d) M.I. Fuks and N.F. Kovalev, "Selective Multi-Channel Feedback," IEEE Trans. Plasma Sci., vol. 30, pp. 1147-1150 (2002).

e) K. Hahn, M. Fuks, and E. Schamiloglu, "Initial Studies of a Long Pulse Relativistic Backward Wave Oscillator Utilizing a Disk Cathode," IEEE Trans. Plasma Sci., vol. 30, pp. 1112-1119 (2002).

f) I.S. Bakim, C.T. Abdallah, and E. Schamiloglu, "Communicating with Microwave-Propelled Sails," accepted for publication in IEEE Antennas and Propagation Magazine (2003).

g) R.L. Wright and E. Schamiloglu, "Space-charge-limited-current in Cylindrical Geometry," submitted to Phys. Plasmas (2003).

2. Papers in Conference Proceedings

a) S.H. Choi and E. Schamiloglu, "Full Power Operation of an Ultra-Compact, Low Voltage Reltron Microwave Source," *Proceedings BEAMS 2002* (Albuquerque, NM, 2002), pp. 311-314.

b) M.I. Fuks, M.B. Goikhman, N.F. Kovalev, A.V. Palitsin, and E. Schamiloglu, "On Measurements of the Basic Parameters of High-Current Relativistic Electron Beams," *Proceedings BEAMS 2002* (Albuquerque, NM, 2002), pp. 235-238.

c) M.I. Fuks, N.F. Kovalev, A.V. Palitsin, and E. Schamiloglu, "Cyclotron Suppression of Pre- and Post-Pulse Radiation from a Relativistic BWO Pulse," *Proceedings BEAMS 2002* (Albuquerque, NM, 2002), pp. 267-270.

d) N.F. Kovalev, M.I. Fuks, and E. Schamiloglu, "Stability of Generation of Relativistic BWO With Reflections in Output Waveguide," *Proceedings BEAMS 2002* (Albuquerque, NM, 2002), pp. 271-274.

e) E. Schamiloglu, "High Power Microwave Sources: Where do we go from here?" *Proceedings 25th International Power Modulator Symposium and 2002*

High Voltage Workshop (Hollywood, CA, 2002), pp. 694-698.

f) M. Fuks and E. Schamiloglu, "Some Possibilities for Single Mode Generation in Oversized Cerenkov Oscillators," *The Papers of Joint Technical Meeting on Plasma Science and Technology and Pulsed Power Technology, IEE Japan* (Proceedings of the Joint Workshop, Kailua-Kona, Hawaii, August 2002), pp. 49-54.

g) D. Georgiev, E. Schamiloglu, C.T. Abdallah, and E. Chahine, "3-D Simulation of Rigid Microwave Propelled Sails using Spin," *Proceedings First International Symposium on Beamed Energy Propulsion* (Huntsville, AL, 2002), AIP Conference Proceedings 664 (Melville, NY, 2003), pp. 336-347.

h) C.T. Abdallah, E. Chahine, D. Georgiev, and E. Schamiloglu, "Dynamics and Control of Microwave-propelled Sails using Delayed Measurements," *Proceedings First International Symposium on Beamed Energy Propulsion* (Huntsville, AL, 2002), AIP Conference Proceedings 664 (Melville, NY, 2003), pp. 348-357.

i) Z. Kancleris, M. Dagys, R. Simniskis, E. Schamiloglu, and F.J. Agee, "Recent Advances in HPM Pulse Measurement using Resistive Sensors," to appear in *Proceedings 14th IEEE International Pulsed Power Conference.*

j) A. Shlapakovski, W. Jiang, and E. Schamiloglu, "Numerical Simulations of an Antenna-amplifier Cherenkov Maser with a Rod Slow Wave Structure Operating in Non-axisymmetric mode, to appear in *Proceedings 14th IEEE International Pulsed Power Conference.*

k) M. Fuks, M. Goikhman, A. Palitsin, N. Kovalev, and E. Schamiloglu, "Improvement of Selective Properties of Waveguide Bragg Resonators," to appear in *Proceedings RF-2003.*

3. Abstracts

a) I.S. Kim, N.F. Kovalev, M.I. Fuks, and E. Schamiloglu, "Diffraction Grating Comprised of Thin Metal Rods with Transverse Gaps, AMEREM 2002 Symposium (Annapolis, MD, June 2002).

b) M. Dagys, Z. Kancleris, E. Schamiloglu, and F.J. Agee, "Recent Advances in HPM Pulse Monitoring using Resisitive Sensors," AMEREM 2002 Symposium (Annapolis, MD, June 2002).

c) E. Schamiloglu, "High Power Microwave Sources," **(Invited Tutorial)**, *IEEE EMC 2003* (Istanbul, Turkey, May 2003).

RECOGNITION

1. Professor Edl Schamiloglu, City of Albuquerque Goodwill Ambassador Award – May 2003.

NEW DISCOVERIES, INVENTIONS, PATENTS

None.